PROCEEDINGS, Twenty-Ninth Workshop on Geothermal Reservoir Engineering
Stanford University, Stanford, California, January 26-28, 2004
SGP-TR-175

IN SITU STRESS, FRACTURE, AND FLUID FLOW ANALYSIS IN WELL 38C-9: AN ENHANCED GEOTHERMAL SYSTEM IN THE COSO GEOTHERMAL FIELD

Judith M. Sheridan[1] and Stephen H. Hickman[2]

[1]GeoMechanics International Inc., Palo Alto, California, USA (e-mail: judith@geomi.com)
[2]U.S. Geological Survey, Menlo Park, California, USA (e-mail: hickman@usgs.gov)

ABSTRACT

Geoscientists from the Coso Operating Company, EGI-Utah, GeoMechanics International, and the U.S. Geological Survey are cooperating in a multi-year study to develop an Enhanced Geothermal System (EGS) in the Coso Geothermal Field. Key to the creation of an EGS is an understanding of the relationship among natural fracture distribution, fluid flow, and the ambient tectonic stresses that exist within the resource in order to design a hydraulic and thermal stimulation of an east-flank injection well, the first step in the creation of a heat exchanger at depth. Well datasets from the east flank of the Coso Geothermal Field are being analyzed to develop an understanding of the relationships between natural fracture distribution, fluid flow, and the ambient tectonic stresses that exist within the resource.

During the second year of this project, wellbore logs and stress data were acquired in a new production well drilled in the Coso Geothermal Field, 38C-9. The image analysis results include the discrimination of natural from drilling induced fractures in wellbore image data, natural fracture characterization, and wellbore failure analysis. A hydraulic fracturing stress test at 3,703 feet TVD was used to constrain a normal faulting and strike-slip faulting stress tensor for this reservoir. The shear and normal stresses resolved on the fracture and fault planes were calculated and used to identify the subset of critically stressed planes that act to maintain permeability within the Coso Geothermal Field.

INTRODUCTION

The east flank of the Coso Geothermal Field is an excellent setting for testing Enhanced Geothermal System (EGS) concepts. Fluid temperatures exceeding 300°C have been measured at depths less than 10,000 feet and the reservoir is both highly fractured and tectonically stressed. However, some of the wells within this portion of the reservoir are relatively impermeable. High rock temperatures, a high degree of fracturing, high tectonic stresses, and low intrinsic permeability are the combination of qualities that define an ideal candidate EGS reservoir. The long-term goal of this five-year project is to develop and evaluate an approach for the creation of an EGS within the east flank of the Coso Geothermal Reservoir.

Barton et al. (1995, 1998) have shown that optimally oriented, critically stressed fractures control permeability in areas of active tectonics. This suggests that critically stressed fracture sets are likely to be responsible for the majority of the geothermal production in the Coso Geothermal Field. A detailed analysis is required in order to develop a geomechanical model of the reservoir, to determine which fractures are optimally oriented and critically stressed for shear failure, and determine their role in reservoir permeability. The geomechanical model includes pore pressure (P_p), uniaxial compressive rock strength (C_0), and the magnitudes and orientations of the principal stresses including the maximum horizontal stress (S_{Hmax}), the minimum horiztonal stress (S_{hmin}), and the vertical stress (S_v). These are derived from in situ pore pressure measurements, laboratory rock strength tests, wireline log data, hydraulic fracturing (minifrac) test results, and observations of wellbore failure. Only through fracture and wellbore failure analyses of image data, correlated petrographic analyses, and identifying critically stressed fault orientations and fault orientations in fluid flow intervals can we then understand the effects of subsequent stimulation experiments on fracture permeability.

We adopted a multi-step approach used in previous studies at Coso and elsewhere (Barton et al., 1997, 1998; Hickman et al., 1998, 2000; Sheridan et al., 2003). We measured the orientation and distribution of fractures in two logged intervals in Coso well 38C-9, the newly drilled production well of the EGS doublet. We developed preliminary constraints on the in situ state of stress based on observations of wellbore failure, the results of a hydraulic fracture test at 3,703 feet true vertical depth (TVD) to obtain S_{hmin}, and stress modeling to constrain the magnitude of S_{Hmax}. All fractures were then analyzed for their proximity to frictional failure using both a strike-slip and normal faulting stress model.

IMAGE DATA ANALYSIS

Electric Micro Imager (EMI) data were acquired in two intervals in well 38C-9, from 690–3,726 feet measured depth (MD) and 5,881–9,408 feet MD. The EMI tool provides good data for detecting macroscopic fractures that intersect the wellbore and cut across lithologic or stratigraphic contacts, allowing for analysis of natural fractures (Figures 1a and 1b) and drilling-induced failure features such as tensile fractures (Figure 1c) and borehole breakouts (Figure 1d). GMI•Imager™, designed specifically for the analysis of digital wellbore image data, was used to interpret natural and drilling-induced features in the EMI image data for the Coso wells.

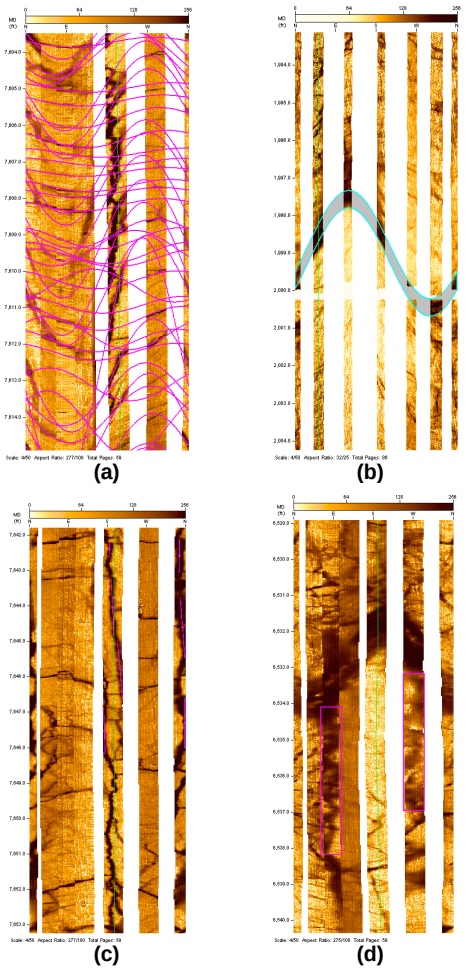

Figure 1. Examples of EMI image data from Coso 38C-9. (a) Natural fractures, (b) fracture with a significant apparent aperture, (c) drilling-induced tensile wall fractures, and (d) borehole breakouts.

Natural Fracture Analysis

Planar features detected in electrical image data are the result of the electrical conductivity contrast between the feature and the host rock and appear as sinusoids on unwrapped 360° views of the image data (e.g., Figure 1a). The true dip, true dip direction, and fracture density for all natural fractures were tabulated (Figures 2a, 2b, 2c, and 3a, 3b, 3c). We also identified a subset of fractures with a significant apparent aperture (Figure 1b) in this well and analyzed their orientations (Figures 2d, 2e, 2f, and 3d, 3e, 3f). The apparent aperture observed in electrical image logs results from a high electrical conductivity contrast that can represent either the presence of a highly conductive fluid (e.g., drilling mud), or a highly conductive vein-filling material resulting from hydrothermal alteration. Thus, at least in some cases, fractures with significant apparent aperture due to mud infiltration may be acting as fluid flow pathways.

Dips of all fractures range from moderate to steep (Figures 1a and 2a). Vertical fractures are observed where the wellbore deviation increases. Dip azimuths are bimodal, ENE to NNW in the shallow interval (Figure 1b) and NE and NW in the deeper interval (Figure 2b).

Dip azimuths of fractures with significant apparent aperture (Figures 1f and 2f) tend to mimic the dip azimuths of the bulk fracture population (Figures 1b and 2b), but they have steeper dips in the deep interval (Figure 3e) when compared with the bulk fracture population (Figure 3a).

Summary plots show true dip (Figure 4) and true dip direction (Figure 5) versus true vertical depth for all wells analyzed in the Coso East Flank EGS project (38A-9, 38B-9, 38C-9, 83-16, and 86-17). A more detailed analysis of these earlier data is presented in Sheridan et al., 2003. A similar fabric is observed in most of the Coso East Flank wells where there are mainly two dip directions (Figure 5), but the dominance of one dip direction over the other varies from well to well and can also vary with depth within a single well.

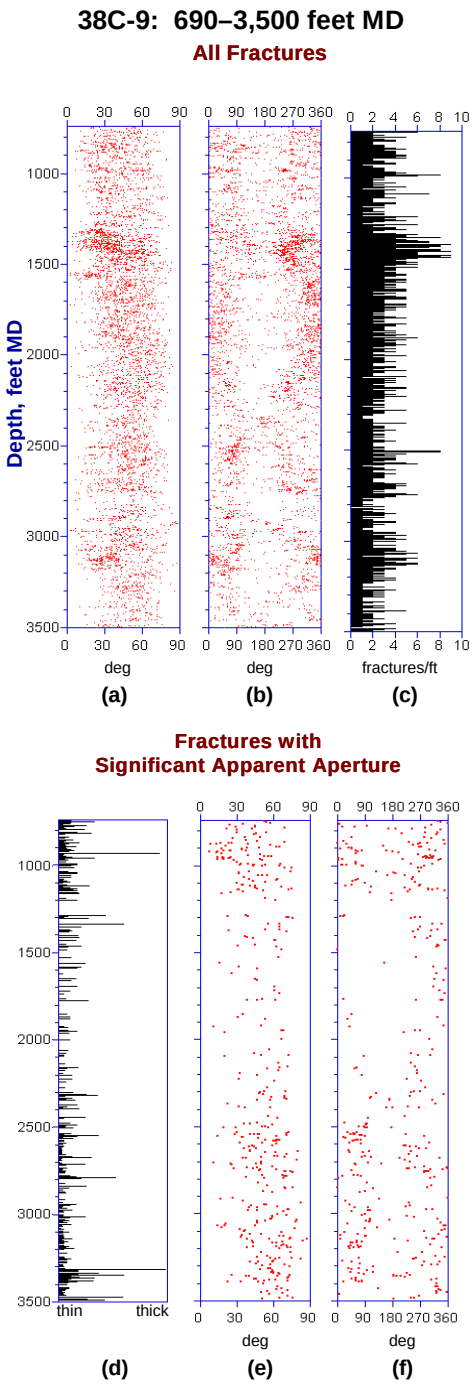

Figure 2. Coso 38C-9 fracture analysis results for the shallow logged interval, 690 to ~3,500 feet MD. (a) True dip, (b) true dip direction, (c) fracture density of all natural fractures. (d) Apparent aperture, e) true dip, f) and true dip direction for fractures with a significant apparent aperture.

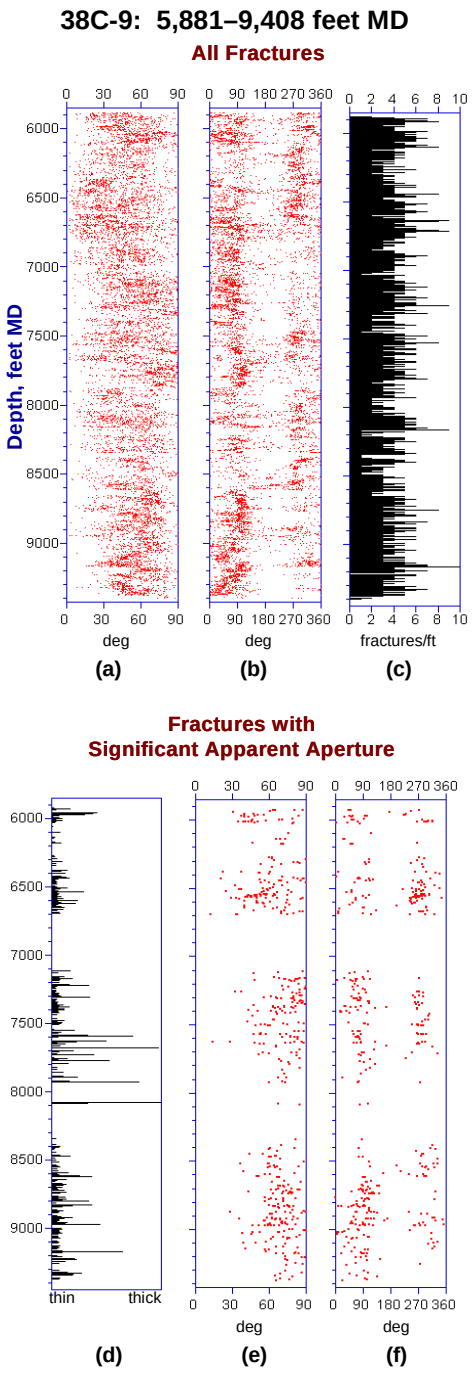

Figure 3. Coso 38C-9 fracture analysis results for the deep logged interval, 5,881–9,408 feet MD. (a) True dip, (b) true dip direction, (c) fracture density of all natural fractures. (d) Apparent aperture, (e) true dip, (f) and true dip direction for fractures with a significant apparent aperture.

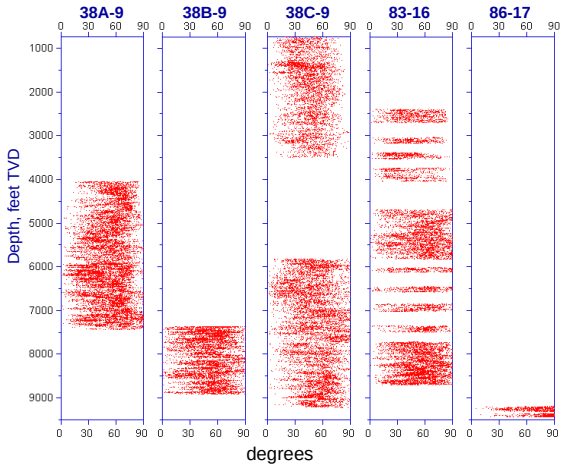

Figure 4. True dip versus true vertical depth for natural fractures in Coso East Flank wells.

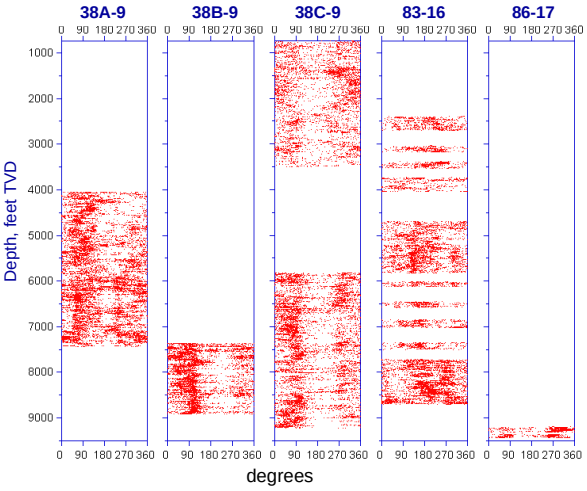

Figure 5. True dip azimuth versus true vertical depth for natural fractures in Coso East Flank wells.

Observations of Borehole Failure

As discussed in Moos and Zoback (1990), drilling-induced tensile fractures occur in the borehole wall along the azimuth of S_{Hmax} where the circumferential hoop stress is negative and exceeds the tensile strength of the rock (Figure 1c). These fine-scale features occur only in the wall of the borehole (due to the localized stress concentration) and do not propagate away from the hole. Vertical tensile fractures are infrequently observed in the shallow log and are more pervasive in the deeper image log in Coso 38C-9.

Stress-induced borehole breakouts occur when the compressive stress concentration around the borehole wall exceeds the rock strength (Figure 1d). The presence, orientation, and severity of failure are a function of the in situ stress field, the wellbore orientation, and the rock strength (e.g., Moos and Zoback, 1990; Peska and Zoback, 1995). In a vertical or near-vertical well in a region where overburden is a principal stress, breakouts may form on opposite sides of the wellbore at the azimuth of S_{hmin}, as this is where the compressive hoop stress is greatest. Only a single breakout was observed in 38C-9.

The results of numerous observations of drilling-induced tensile fractures and a single breakout were used to determine that the S_{Hmax} azimuth for 38C-9 is N11° ±17° (Figure 6).

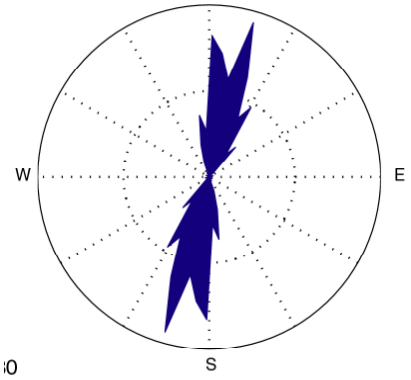

Figure 6. 38C-9 S_{Hmax} azimuth is N11° ±17° based on failure analysis of EMI image logs.

Figure 7 compares the S_{Hmax} azimuth from 38C-9 against the S_{Hmax} azimuths for previously analyzed Coso East Flank wells (Sheridan et al, 2003). The S_{Hmax} azimuth results for 38C-9 and 38A-9 are quite similar to one another, but are rotated counterclockwise relative to the S_{Hmax} azimuth observed in wells 38B-9 and 83-16.

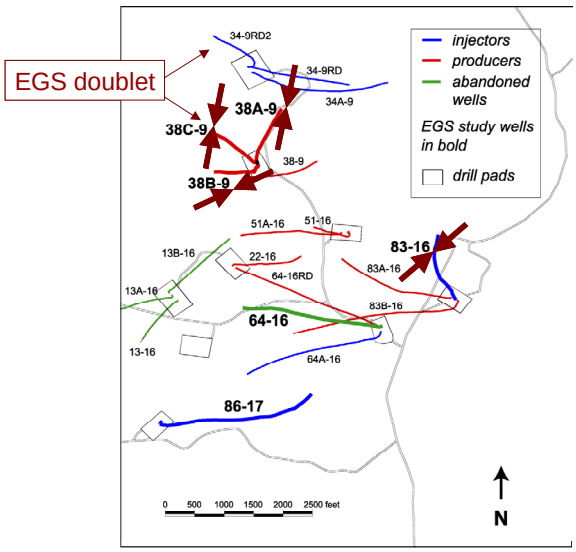

Figure 7. Coso East Flank S_{Hmax} azimuths.

HYDRAULIC FRACTURING STRESS MEASUREMENT

As done in other geothermal fields (see Hickman et al., 1998, 2000), following cementation of the casing at a depth of 3,684 feet MD, a 57-foot long pilot hole was drilled out the bottom of the well in which to conduct the hydrofrac test. The entire casing string was pressurized to induce a hydraulic fracture in the uncased pilot hole. Repeated pressurization cycles were then employed to extend this fracture away from the borehole. Pressures and flow rates were measured at the surface and a high-accuracy, temperature-compensated quartz pressure gauge was suspended 42 feet above the center of the test interval to provide a continuous record of downhole pressure during this test.

Following Hickman and Zoback (1983), the magnitude of the least horizontal principal stress, S_{hmin}, was determined from the instantaneous shut-in pressure (ISIP), or the pressure at which the pressure-time curve departs from an initial linear pressure drop immediately after the pump is turned off and the well is shut in (Figures 8a and 9). The interpretation of the 38C-9 hydrofrac test was complicated by the fact that a highly permeable interval of the formation was encountered during drilling of the 57-foot pilot hole, causing rapid fall off in the standing water level in the well both prior to conducting the hydrofrac and between pumping cycles (Figure 8b) and rapid pressure decays during hydrofrac shut in periods (Figure 8a). In spite of this rapid decay in shut-in pressure, by expanding the time scale we were able to make six determinations of the ISIP (Figure 9). As discussed in Hickman et al. (1988), the observation that the values determined for ISIP were relatively repeatable and insensitive to variations in pump rate immediately preceding shut in (Figure 8a) indicates that viscous pressure losses within the hydraulic fracture near the borehole had a negligible effect on the ISIP values and that we are obtaining a good measure of S_{hmin} magnitude. Thus, analysis of the hydraulic fracturing data from well 38C-9 shows that the magnitude of S_{hmin} at 3,703 feet TVD is 2,645 ±77 psi (Figure 10). Using an estimated granite density of 2.63 gm/cm^3 indicates that the magnitude of S_{hmin} at this depth is about 0.63 of S_v. This is at the high end of the range observed within the producing portions of the Dixie Valley Geothermal Field, where S_{hmin}/S_v ranges from 0.45–0.62 at depths of 0.4–2.5 km (Hickman et al., 1998, 2000).

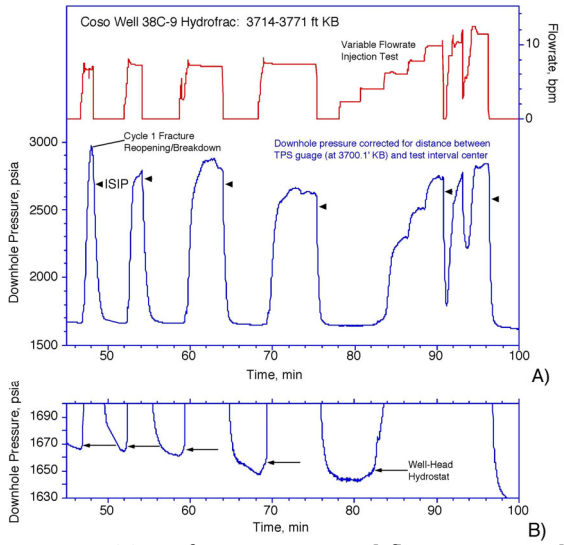

Figure 8. (a) Surface pressure and flow rate records from the hydraulic fracturing test conducted in well 38C-9. (b) Expanded scale showing rapid drop in borehole water level between pumping cycles due to high test-interval permeability.

Downhole pumping pressures were recorded during a stepwise change in flow rate in the last cycle of this test in an attempt to detect changes in the permeability of the test interval resulting from closure of the hydraulic fracture near the wellbore. However, interpretation of this portion of the test is ambiguous owing to the very high test-interval permeability encountered and the currently low reservoir pressure at this depth.

In a hydraulic fracturing test, the magnitude of S_{Hmax} is sometimes determined using a fracture initiation, or breakdown, criteria derived for pure mode I tensile fractures initiating in intact (i.e., unfractured) rock along the S_{Hmax} direction. However, as was the case in similar tests conducted in the Dixie Valley Geothermal Field (Hickman et al. 1998, 2000), borehole image logs conducted in well 38C-9 show pervasive pre-existing fractures at a variety of orientations. Thus, as described below, we placed upper bounds on the magnitude of S_{Hmax} using our measured S_{hmin} value and the near-absence of borehole breakouts in this well.

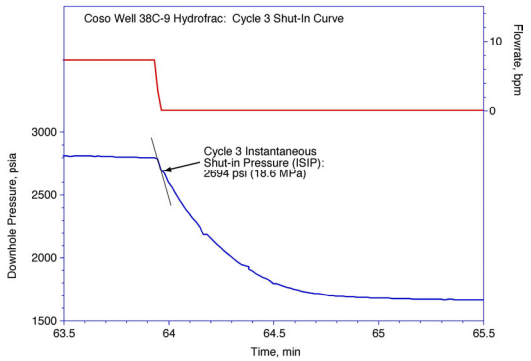

Figure 9. Expanded view of shut-in pressure decay at the end of cycle 3, showing how the instantaneous shut-in pressure was determined.

CONSTRAINTS ON S_{HMAX} FROM BREAKOUT ANALYSIS

Given that only a single borehole breakout was observed in well 38C-9, upper bounds to the magnitude of S_{Hmax} were obtained using the S_{hmin} magnitude measured at 3,703 feet together with theoretical models for breakout formation (e.g., Moos and Zoback, 1990). These models predict that borehole breakouts will initiate along the azimuth of S_{hmin} whenever the maximum effective circumferential stress, $\sigma_{\theta\theta}^{max}$, at the borehole wall exceeds the compressive rock strength, C_0; i.e.,

$$\sigma_{\theta\theta}^{max} = 3S_{Hmax} - S_{hmin} - P_p - P_m \geq C_0 \qquad (1)$$

where P_p is the formation pore pressure and P_m is the mud pressure exerted on the borehole wall during drilling. In this analysis we used preliminary rock strength measurements on Coso reservoir rocks (using cores taken from shallower wells) by TerraTek, Inc., which indicated C_0 of approximately 22,000 psi, together with a value of C_0 = 15,000 psi, which is at the low end of that observed for most granites (Lockner 1995). We used Equation 1 to place an upper bound on S_{Hmax} at a depth of 3,703 feet, the depth of our hydraulic fracturing test, and at 7,750 feet, the target depth for the EGS injection well, 34-9RD2 (see Figure 7). For the shallowest bound we used the S_{hmin} magnitude as measured directly from our hydraulic fracturing test. For the deeper bound we extrapolated the measured S_{hmin} value to depth assuming a constant ratio of effective principal stresses, as appropriate for ambient differential stress levels being controlled by frictional failure. This analysis indicates that S_{Hmax} is equal to or less than the critical values required for frictional failure on optimally oriented strike-slip faults (Figure 10). Taken together, our hydraulic fracturing stress measurement of S_{hmin} and these upper bounds to S_{Hmax} are consistent with a stress regime at this site that is transitional between strike-slip faulting ($S_{hmin} < S_v < S_{Hmax}$) and normal faulting ($S_{hmin} < S_{Hmax} < S_v$; see Figure 10).

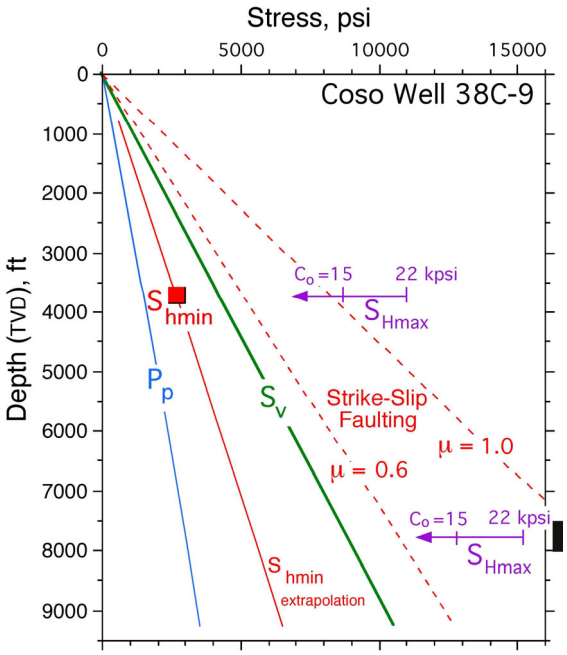

Figure 10. Results of hydraulic fracturing stress measurement (S_{hmin}) and upper bounds on S_{Hmax} from failure analysis in well 38C-9. Dashed lines indicate the range of S_{Hmax} magnitudes where strike-slip faulting would be expected given the observed magnitude of S_{hmin} for coefficients of friction of 0.6–1 (after Byerlee, 1978; see Hickman et al., 1998). P_p and failure envelope were drawn assuming that the pre-production water table was in hydrostatic equilibrium with the surface under present-day thermal conditions. S_{Hmax} bounds were from the general absence of breakouts, assuming minimum C_0 shown (see text). The black bar along the right vertical axis denotes the target depth for the EGS injector, 349RD2.

COULOMB FAILURE ANALYSIS

GMI•MohrFracs™ predicts critically stressed fracture orientations using Mohr-Coulomb faulting theory to calculate the effective shear stress and normal stresses acting on each fracture plane given the orientations and magnitudes of the three principal stresses and the formation fluid pressure. Barton et al. (1995, 1998) have shown that optimally oriented, critically stressed fractures control permeability in areas of active tectonics. This suggests that critically stressed fracture sets are likely to be responsible for

the majority of the geothermal production in the Coso Geothermal Field.

Using S_{hmin} extrapolated from the value measured in the hydraulic fracturing test (Figure 10), we used two end-member stress states to bracket the possible range of S_{Hmax} values. These are a transitional normal to strike-slip faulting model ($S_{hmin} < S_{Hmax} = S_v$) and a strike-slip faulting model ($S_{hmin} < S_v < S_{Hmax}$) where S_{Hmax} is fixed along the $\mu = 0.6$ failure line shown in Figure 10. For each of these models we then calculated the ratio of shear to effective normal stress acting on each of the fractures observed in 38C-9 and displayed the results in lower hemisphere, stereographic projections of poles to these fracture planes (Figure 11).

In these calculations we used the post-production pore pressure, which resulted in very few critically stressed fractures under current reservoir conditions in Coso 38C-9. We then calculated the amount of reservoir pressure increase needed to trigger frictional failure (slip) on fractures observed in the EMI logs for both of the stress models used. The strike-slip faulting model requires smaller excess pressures (less than 500 psi above ambient) to initiate slip on properly oriented fractures (Figure 11b), whereas the transitional normal faulting to strike-slip model requires between 500 and 1000 psi above ambient to initiate slip on properly oriented fractures (Figure 11a).

In well 38C-9, the orientation of S_{Hmax} is N11°E. As a result, critically stressed faults defined by the transitional normal faulting to strike-slip faulting model strike NNE–SSW and dip approximately 60° either towards the WNW or towards the ESE (Figure 11a). Critically stressed fractures in the strike-slip faulting model either dip steeply to the east with strikes that range from NE to NW, or they dip steeply to the west with strikes that range from SW to SE (Figure 11b).

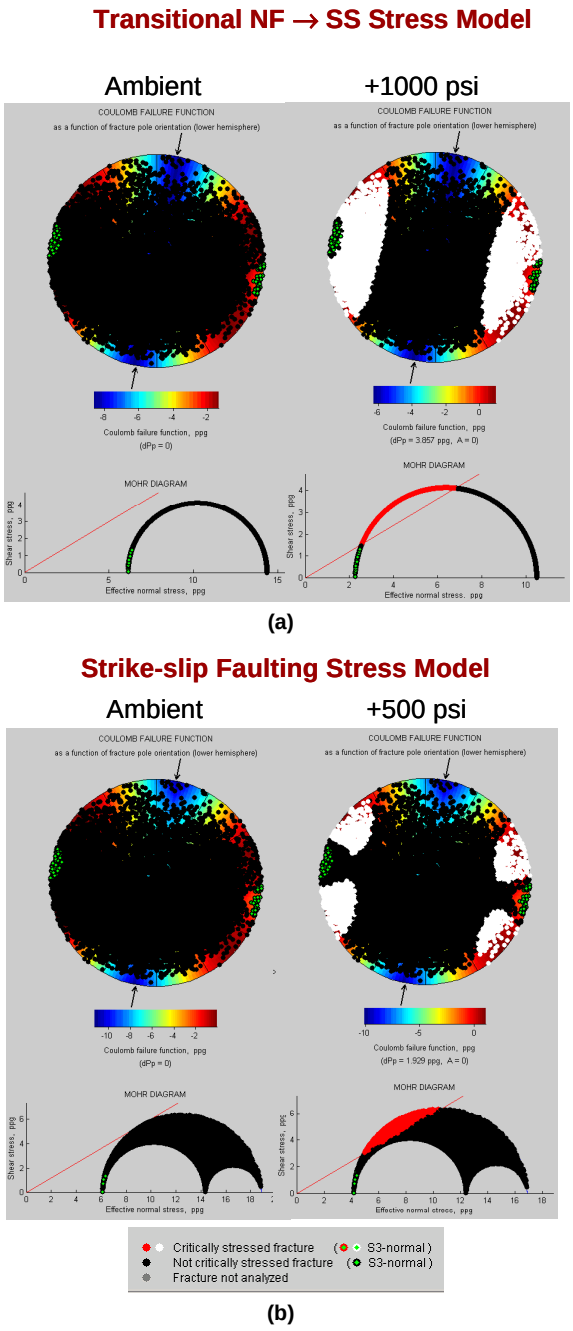

Figure 11. GMI•MohrFracs analysis results using (a) transitional normal to strike-slip faulting stress model and (b) strike-slip faulting stress model applied to all fractures measured in well 38C-9. The white dots denote fractures that are critically stressed for shear failure for coefficients of friction of 0.6 (after Byerlee, 1978). The terms ambient and +500, +1000 psi denote the amount of excess fluid pressure applied above current, post-production ambient values.

CONCLUSIONS

Coso well 38C-9 is the first drilled of two new wells planned for an Enhanced Geothermal System in the Coso East Flank area. 38C-9 datasets were analyzed to characterize fracture orientations and stress magnitudes and orientations in order to identify the subset of critically stressed planes that act to maintain permeability within the Coso Geothermal Field. These results will also be incorporated in the design of the EGS reservoir injection and stimulation program for the East Flank. The image analysis for 38C-9 shows a preponderance of moderate to steeply dipping fractures, dipping towards either the northeast or northwest, similar to results from other wells in the area. The orientation of drilling-induced tensile fractures and a single borehole breakout indicate an S_{Hmax} azimuth of 11º ±17º in well 38C-9. This is parallel to the S_{Hmax} azimuth observed in well 38A-9, but differs from that observed in both southern wells, 38B-9 and 83-16. Hydraulic fracturing stress test results show that the magnitude of S_{hmin} is relatively low (about 0.63 of the vertical stress) but slightly above that predicted for normal faulting failure. However, borehole failure analysis and simple frictional faulting theory indicate that this value of S_{hmin} and approximate bounds on S_{Hmax} are consistent with crustal strength being controlled by strike-slip faulting. Plans to run a hydraulic fracturing stress test in a deeper interval in 34-9RD2, the second well in the EGS doublet, will constrain the stress model further. Fracture failure analyses using the improved Coso stress model indicate that normal faulting failure will not occur under ambient conditions, but can be induced through increases in reservoir pressure in excess of 500 psi. Strike-slip failure can be induced by lesser increases in reservoir pressure.

REFERENCES

Barton, C. A., Zoback, M. D. and Moos, D. (1995), "Fluid flow along potentially active faults in crystalline rock," *Geology*, 23 (8), 683–686.

Barton, C. A., Moos, D. and Zoback, M. D. (1997), "In situ stress measurements can help define local variations in fracture hydraulic conductivity at shallow depth," *The Leading Edge*, 1,653–1,656.

Barton, C. A., Hickman, S., Morin, R., Zoback, M. D. and Benoit, D. (1998), "Reservoir-scale fracture permeability in the Dixie Valley, Nevada, Geothermal Field," *Proceedings 23rd Workshop on Geothermal Reservoir Engineering*, Stanford Univ., 299–306.

Byerlee, J. (1978), "Friction of rocks," *Pure and Applied Geophysics*, 116, 615–626.

Jaeger, J. C. and Cook, N. G. W. (1979), "Fundamentals of Rock Mechanics (Third Edition)," New York, Chapman and Hall, 28–30.

Hickman, S. H. and Zoback, M. D. (1983), "The interpretation of hydraulic fracturing pressure-time data for in-situ stress determination," in *Hydraulic Fracturing Measurements*, edited by M. D. Zoback and B. C. Haimson, National Academy Press, Washington, D.C., 44–54.

Hickman, S., Zoback, M. D. and Healy, J. H. (1988), "Continuation of a deep borehole stress measurement profile near the San Andreas Fault, I: Hydraulic fracturing stress measurements at Hi Vista, Mojave Desert, CA," *Journal of Geophysical Research*, *93*, 15,183–15,195.

Hickman, S., Zoback M. D. and Benoit R. (1998), "Tectonic controls on reservoir permeability in the Dixie Valley, Nevada, geothermal field," *Proceedings 23rd Workshop on Geothermal Reservoir Engineering*, Stanford Univ., 291–298.

Hickman, S., Zoback, M. D., Barton, C., Benoit, R., Svitek, J. and Summers R. (2000), "Stress and permeability heterogeneity within the Dixie Valley geothermal reservoir: Recent results from well 82-5," *Proceedings 25th Workshop on Geothermal Reservoir Engineering*, Stanford Univ., 256–265.

Lockner, D. (1995), "Rock Failure," in *Rock Physics and Phase Relations: A Handbook of Physical Constants*, T. Ahrens (ed.), American Geophysical Union Reference Shelf 3, 127–147.

Moos, D. and Zoback, M. D. (1990), "Utilization of Observations of Well Bore Failure to Constrain the Orientation and Magnitude of Crustal Stresses: Application to Continental, Deep Sea Drilling Project, and Ocean Drilling Program Boreholes," *J. Geophys. Res.*, 95, 9305–9325.

Peska, P. and Zoback, M. D. (1995), "Observations of borehole breakouts and tensile wall fractures in deviated boreholes: A technique to constrain in situ stress and rock strength," *Journal of Geophysical Research, 100*, 12791-12811.

Sheridan, J., Kovac, K., Rose, P. E., Barton, C., McCulloch, J., Berard, B., Moore, J., Petty, S. and Spielman, P. (2003), "In situ stress, fracture and fluid flow analysis-East Flank of the Coso Geothermal Field," *Proceedings 28th Workshop on Geothermal Reservoir Engineering*, Stanford Univ., 34-49.